# A Capacitive Coupling Technique to Mitigate Frequency Mismatch Effects in MEMS Resonators

Luca Colombo*, Giuseppe Michetti*, Pietro Simeoni*, Mary E. Galanko Klemash†, Sarah S. Bedair†, and Matteo Rinaldi*
*SMART Center, Northeastern University, Boston MA, USA
†U.S. Army Combat Capabilities Development Command - Army Research Laboratory, Adelphi MD, USA

***Abstract*—In this paper, a coupling technique based on series loading of arrays of frequency mismatched MEMS resonators is presented. This method exploits the poles coupling that is induced by interfacing a multi Butterworth-Van Dyke (mBVD) model in series with a capacitor. As a result, a single, spurious-free, high quality factor ($Q_s$) peak is generated at a tunable frequency close to the natural resonance of the system. Furthermore, this method is insensitive to the number of spurious modes, to their frequency mismatch, and to the Figure of Merit ($FoM$, defined as the product between $Q_s$ and the electromechanical coupling $k_t^2$) of the arrayed resonators. In the first section of this work, a simple analytical model describing the technique is presented, and its validity is verified via numerical simulations and direct measurements. In the second section, the technique is used to extract the average $Q_s$ of arrays of mismatched elements via a numerical approach. In the third and last section, it is verified that coupled arrays of mismatched elements retain their high quality factor when implemented in cutting edge applications such as high passive gain inductorless matching networks.**

***Index Terms*—MEMS; Resonators; Microacoustic; Modeling**

## I. Introduction

MICROELECTROMECHANICAL Systems (MEMS) have been key-enabling components in modern electronics systems, including radio frequency (RF) filters [1], microphones [2], accelerometers [3], oscillators [4], and gyroscopes [5]. Recent innovations in the field include, but are not limited to, piezoelectric micromachined ultrasonic transducers (pMUTs) [6], and MEMS-based matching networks (MN) in which resonators are implemented in place of on-chip or discrete inductors to provide for large passive voltage amplification and narrowband filtering in Internet of Things (IoT) nodes [7]. As devices performance improvements are expected to further advance radio frequency (RF) applications state-of-the-art, conventional MEMS cannot fulfill the arising technological challenges. For example, matching networks implementing resonators as inductive elements demand Figure of Merits ($FoM$), defined as the product between the quality factor at resonance ($Q_s$) and the electromechanical coupling ($k_t^2$), larger than the ones of widely, commercially available resonators, namely Surface Acoustic Wave (SAW) and Film Bulk Acoustic Resonators (FBARs). One way of enabling low motional resistance ($R_m$) devices is to maximize the $Q_s$ of a single resonator by geometry optimization [8], and subsequently array them in parallel to attain the desired static capacity ($C_0$). This approach is particularly useful when low $C_0$ densities are in place (*e.g.*, due to lateral field excitation). However, this technique requires a precise control of the fabrication process, since frequency mismatch between array elements (usually between tens and few hundreds ppm) is known to degrade the quality of the resonance peak [9].

In this paper, a capacitive coupling technique to to compensate for the resonance frequency mismatch between arrays of microacoustic resonators is presented. In the first section, an analytical model of the coupling technique is derived for the case of two parallel devices with high $FoM$ and resonant frequency mismatch ($\Delta$) close to zero. The model is then validated numerically for a larger frequency mismatch, an arbitrary number of arrayed resonators, and for lower $FoM$ devices. Finally, the coupling technique is verified on a fabricated X-cut Lithium Niobate (LN) array of resonators. In the second section, it is demonstrated that the coupling technique does not introduce $Q_s$ degradation over a large range of capacitance values. It is also showed that this technique can be used to extract the average quality factor of an array of mismatched elements. In the third and last section, it is verified that the capacitive coupling does not degrade the passive voltage amplification obtained when the resonators array is used as an inductor-less matching network.

## II. Modeling and Experimental Validation

The electrical behavior of a 1-port piezoelectric MEMS resonator is, to a first approximation, captured by the Butterworth-

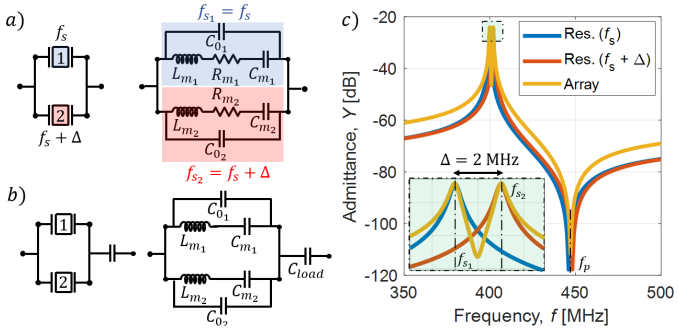


Fig. 1. a) Modeling of an array consisting of two identical, mismatched resonators operating at $f_{s_1}$ and $f_{s_2}$. The resonator electrical behavior is captured by a Butterworth-Van Dyke (BVD) model. Resonator 1 is highlighted in blue, while resonator 2 is highlighted in red; b) Simplified coupled array modeling once neglecting the motional resistances; and c) Simulated admittance ($Y$) of an array of two identical mismatched resonators showcasing a double peak ($Q_s$ = 1,000, $k_t^2$ = 0.3, $C_{0_i}$ = 100 fF, $f_s$ = 400 MHz, and $\Delta$ = 2 MHz).

Van Dyke (BVD) model (Fig.1a). The model consists in a series resonant branch characterized by a motional resistance, inductance, and capacitance ($R_m$, $L_m$, and $C_m$ respectively) in parallel to a static branch ($C_0$) [10]. For the sake of simplicity, the coupling model is developed for the case of two parallel resonators, characterized by identical $Q_s$, $k_t^2$, and $C_0$, and a slight misalignment ($\Delta$) between their natural frequencies of resonance ($f_s$). In case of high $Q_s$, the impact of $R_{m_1}$ and $R_{m_2}$ on $f_s$ can be neglected, leading to the simplified model shown in Fig.1b. An example of admittance response of two arrayed mismatched resonators operating around 400 MHz and mismatched by a $\Delta$ of 2 MHz is reported in Fig.1c. The equivalent admittance of the array ($Y_p$) shown in Fig.1b can be expressed as:

$$Y_p = Y_1 + Y_2 = j\omega(C_{0_1} + C_{0_2}) + \frac{j\omega C_{m_1}}{(1 - \frac{\omega^2}{\omega_{s_1}^2})} + \frac{j\omega C_{m_2}}{(1 - \frac{\omega^2}{\omega_{s_2}^2})} \quad (1)$$

where $\omega_{s_1} = 2\pi f_s$ and $\omega_{s_2} = 2\pi(f_s + \Delta)$, or $\omega_{s_2} = \omega_{s_1} + \delta$. $\delta$ is the angular frequency mismatch ($\delta = 2\pi\Delta$), while $C_0$ is the sum of $C_{0_1}$ and $C_{0_2}$. By loading the array with an arbitrarily large series capacitor ($C_{load}$), as in Fig.1b, the equivalent admittance of the system ($Y$) becomes:

$$Y = \left( \frac{1}{Y_p} + \frac{1}{j\omega C_{load}} \right)^{-1} \quad (2)$$

By rearranging Eq.2 and setting the denominator equal to zero, it is possible to write the equation that determines the poles, or resonances, of the system as:

$$\omega^4 - \omega^2(\omega_{RF_1}^2 + \omega_{RF_2}^2) + \omega_{RF_1}^2\omega_{s_2}^2 + \omega_{RF_2}^2\omega_{s_1}^2 - \omega_{s_1}^2\omega_{s_2}^2 = 0 \quad (3)$$

where $\omega_{RF_1}$ and $\omega_{RF_2}$ are the pulled or operating resonant angular frequencies of the resonators if they were individually interfaced with $C_{load}$ without being arrayed. These frequencies and the frequency pulling factor ($\gamma$) can be expressed, respectively, as:

$$\omega_{RF_i} = \frac{\omega_{s_i}}{\gamma} \quad (4)$$

$$\gamma = \sqrt{\frac{C_0 + C_{load}}{C_0 + C_{load} + C_{m_i}}} \quad (5)$$

In other words, when a resonator is interfaced in series with a capacitor, $f_{RF}$ shifts from the antiresonance ($f_p$) toward the resonance ($f_s$) with increasing $C_{load}$ [8]. For $\delta$ approaching zero, it is possible to assume that $\omega_{s_2} \approx \omega_{s_2} \approx \omega_s$, $C_{m_1} \approx C_{m_2} \approx C_m$, and thus $\omega_{RF_1} \approx \omega_{RF_2} \approx \omega_{RF}$. Under these assumptions, Eq.3 can be simplified, and two roots can be analytically calculated:

$$\bar{\omega}_{RF_1} = \omega_s \quad (6)$$

$$\bar{\omega}_{RF_2} = \bar{\omega}_{RF} = \omega_{RF}\sqrt{2 - \gamma^2} = \omega_s\sqrt{\frac{2 - \gamma^2}{\gamma^2}} \quad (7)$$

The results from Eq.6 and 7 hint that the capacitive coupling induces a frequency pulling, merging the response of the two frequency mismatched resonators into a single, pulled resonant frequency ($\bar{\omega}_{RF}$) close to $\omega_{RF}$. Interestingly, a second peak close to $\omega_s$ emerges due the poles coupling. These analytical results are supported by numerical simulations on ideal resonators (Fig.2a), where an array of two frequency mismatched resonators is pulled for different values of $C_{load}/C_0$ ratios ($\alpha$). While $\bar{f}_{RF_2}$ moves freely between the antiresonance and the resonance for different values of $\alpha$, $\bar{f}_{RF_1}$ is tied around $f_s$. As expected, the numerical extracted values of the frequencies of operation vary with $\Delta$ (Fig.2b), and converge to the analytical solution for $\Delta \to 0$. The numerical analysis shows that this coupling technique also works for an arbitrarily large number of modes (Fig.3a) and for devices exhibiting low Figure of Merit (Fig.3b). The model is finally validated on a 3-element array

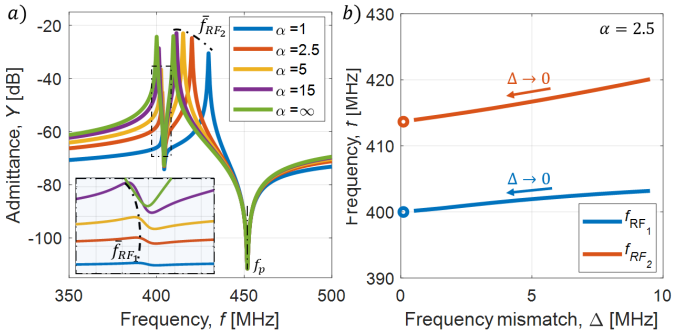


Fig. 2. a) Simulated admittance response of the ideal resonator reported in Fig.1c when coupled to a series capacitor with different values of $C_{load}$ = [0.2 0.5 1 3 500] pF. The legend reports the value of $C_{load}$ normalized over $C_0$ ($\alpha$). As expected, $\bar{f}_{RF_2}$ decreases when $\alpha$ increases, while $\bar{f}_{RF_1}$ remains close to $f_s$ (inset); and b) $\bar{f}_{RF_1}$ and $\bar{f}_{RF_2}$ as a function of frequency mismatch ($\Delta$) for $\alpha$ = 2.5. The numerical results converge to the analytical values (blue and red dot, respectively) when $\Delta \to 0$.

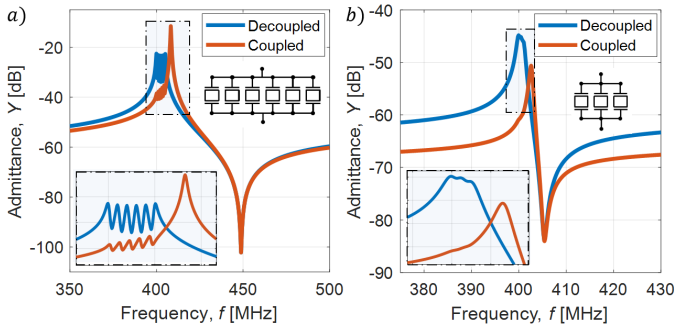


Fig. 3. a) Simulated natural and coupled response of a 6-element array with high $FoM$ ($Q_s$ = 1,000, $k_t^2$ = 0.3, and $C_{0_i}$ = 100 fF) resonators operating around 400 MHz. The frequency spacing ($\Delta$) is 1 MHz. After series capacitive coupling ($\alpha$ = 0.8), a single, clean, and high-$Q$ peak arises far from resonance due to pulling. The other 5 modes can be traced close to $f_s$; and b) Simulated natural and coupled response of a 3-element array with low $FoM$ ($Q_s$ = 500, $k_t^2$ = 0.03, and $C_{0_i}$ = 100 fF) resonators operating around 400 MHz. The frequency spacing ($\Delta$) is 0.5 MHz. Even in this case, a single peak is generated via series capacitive coupling ($\alpha$ = 1.6)

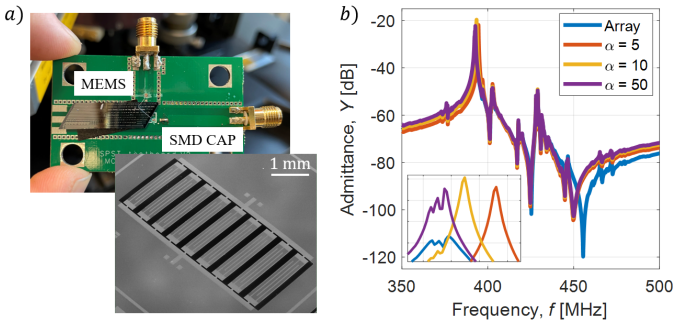


Fig. 4. a) Experimental setup for the verification of series capacitive coupling on an array of 3 parallel, X-cut lithium niobate resonators. The resonator ($C_0 \approx 100fF$) is bonded to the pads of a PCB and a SMD capacitor is soldered in series to it. In the inset, an SEM image of a LN resonator is showed; and b) Measured admittance ($Y$) of the array for different values of $\alpha$ (corresponding to a $C_{load}$ of 1, 2, and 5 pF). A clean peak is achieved for $\alpha$ <50.

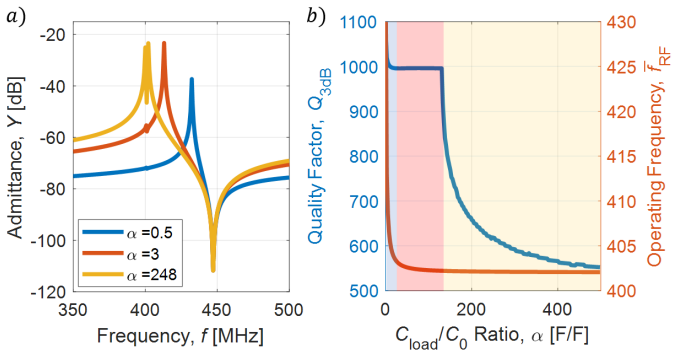


Fig. 5. a) Simulated admittance coupled response of the ideal array of mismatched resonators introduced in Fig.1c. For low and intermediate levels of coupling ($\alpha \sim$ tens) a clean peak is achieved, while for larger level of couplings ($\alpha \sim$ hundreds) the coupling loses effectiveness and a split peak resurfaces; and b) Extracted $Q_{3dB}$ as a function of $\alpha$ for the array reported in Fig.1c. Three regions can be identified: 1) a blue region ($\alpha \sim 1$) in which $Q$ is overestimated; 2) a red region ($1<\alpha<100$) in which $Q$ is correctly extracted; and 3) a yellow region ($\alpha>100$) in which the extracted $Q$ gets deteriorated due to the proximity of the pulled resonance peak. This last region is the region in which the split peak resurfaces due to poor coupling.

of 30° YZ X-cut 2 µm Lithium Niobate (LN) array resonators fabricated on high resistivity silicon as in [7]. The resonator is bonded to a test PCB board, and different SMD capacitors (1, 2, and 5 pF) are soldered in series to it (Fig.4a). The $S$-parameters of the device are then recorded on a Keysight N5221A PNA and later converted to $Y$-parameters via software. Experimental results show that it is possible to obtain spurious-free, single-peak responses (Fig.4b) for specific values of $\alpha$, as long as the pulled operating frequency ($\bar{f}_{RF}$) falls far enough from the natural frequencies of the mismatched elements. This means that a maximum $C_{load}$, and thus $\alpha$, maximum value exists, beyond which the resonator behaves as it was not being pulled by the capacitor (since the capacitance impedance $Z_{load} \to 0$ for $\alpha \to \infty$).

## III. Impact of Coupling on $Q_s$

An interesting application of this coupling technique is quality factor extraction from arrays of mismatched elements, or devices showcasing spurious modes close to the resonance peak. In this section, the method is validated on an ideal array with $Q_s$ = 1,000 (as in Fig.1c), and then used to extract the quality factor of an array of 13 X-cut LN resonators.

Assuming an ideal coupling capacitor, for low and intermediate values of $\alpha$ (up to few tens), the method proves its effectiveness in generating a spurious-free, pulled response far from resonance (Fig. 5a, blue and red curves). However, for larger values of $\alpha$ (larger $C_{load}$), the coupling is weakened by the impedance decrease of the load, which corresponds to a short circuit load for $\alpha \to \infty$ (yellow curve).

By sweeping $\alpha$ while simultaneously recording the main peak quality factor with the half-power or 3-dB method ($Q_{3dB}$), it is possible to identify three regions, as in Fig.5: 1) for $\alpha$ <1 (blue region), the quality factor is slightly overestimated; 2) for $\alpha$ >1 and <of 150 (red region), $Q_{3dB}$ plateaus at the exact value of the superimposed $Q_s$; 3) for $\alpha$ >150 (yellow region), $Q_{3dB}$ is drastically reduced and decays as $\alpha$ increases, due to the arise of the split peak (as in Fig.5).

In a circuit simulation, the effect of this technique can be observed by adding an ideal capacitor in series to the measured

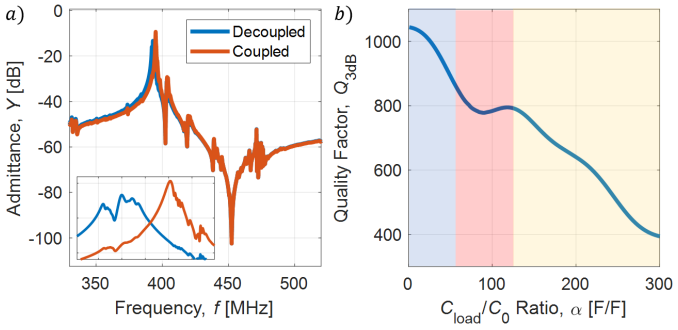


Fig. 6. a) Natural and coupled response of a fabricated 13-element X-cut LN array of resonators ($C_0$ = 2.2 pF, $C_{load}$ = 18 pF, and $\alpha = 8$). The coupling technique allows the extraction of a clean peak even in the presence of several spurious modes; b) Extracted $Q_3dB$ as a function of $\alpha$. Like in Fig.5b, there is a stationary region in which the average $Q$ of the arrayed elements can be extracted (red region). The average extracted quality factor for the device under examination is around 800. Since LN resonators have usually homogeneous quality factor [8], it is reasonable to assume that $Q_s$ approaches the $Q$ of the array.

$Y$-parameters of a resonators array, as shown in Fig.6. In this case, a 13-element 2 µm X-cut LN array is used to benchmark the coupling method. The measured and coupled ($C_0$ = 2.2 pF, $C_{load}$ = 18 pF, and $\alpha$ = 8) admittances of the device are reported in Fig.6a, which shows a clear peak despite the presence of several spurious modes. By sweeping $\alpha$, it is possible to extract a curve (Fig.6) similar to the one reported for the ideal resonator. In this case, the region of $Q_s$ over-estimation is larger (up to $\alpha$ = 50), likely due to the presence of several in-band spurious modes, while a relatively flat band can be identified when $\alpha$ varies between 50 and 120. According to this analysis, the average extracted $Q_s$ of the array elements is around 800 (Fig.6b). As a comparison, the $Q_{3dB}$ of the measured admittance ($\alpha = \infty$) provides an underestimated value around 400.

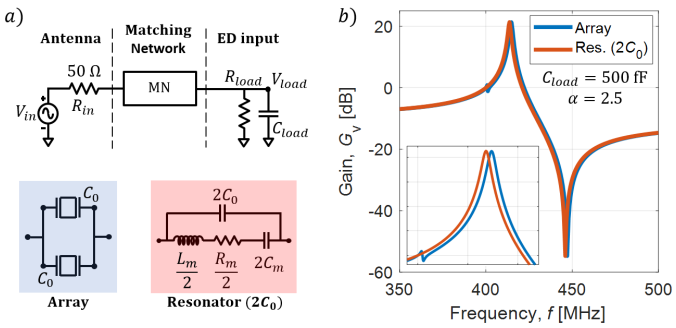


Fig. 7. a) Example of a radio frequency front end (RFFE) implementing a series arrays of resonators as matching network (MN). The case of two identical, mismatched resonator (blue) and single resonator with double static capacitance (red) are compared. Virtually, without frequency mismatch the devices should have the same characteristic response; and b) Simulated gain for a $C_{load}$ of 500 fF. The frequency mismatch induces a slight frequency shift in the array, and introduces a spurious, negligible response around 400 MHz.

## IV. Impact of Coupling on Gain

Recently, the implementation of high $FoM$ microacoustic piezoelectric resonators in radio frequency front ends (RFFE) gained popularity due to the significantly higher passive voltage amplification and filtering performance compared to on-chip or discrete inductors-based matching networks [11]. The coupling technique described in this paper can be used to demonstrate that mismatched arrays of resonators do not impact the gain provided in a MN for a given $C_{load}$. This capacitance can either be the envelope detector (ED) load itself, or an additional series coupling capacitor placed between the matching network and $C_{load}$.

Two ideal devices are investigated (Fig.7a): an array of two mismatched elements (in blue, $Q_s$ = 1,000, $k_t^2$ = 0.3, $C_{0_i}$ = 100 fF, $f_s$ = 400 MHz, and $\Delta$ = 2 MHz) and a single resonator with identical characteristics, but doubled static capacitance ($C_0 = 2C_{0_i}$ = 200 fF). The passive voltage amplification (or gain, $G_v$) is then simulated according to:

$$G_v = |\frac{V_{load}}{V_{in}}| = |\frac{Z_{load}}{Z_{load} + R_{in} + \frac{1}{Y_p}}| \tag{8}$$

where $V_{load}$ is the voltage at the output node, $V_{in}$ the voltage source, and $R_{in}$ the characteristic impedance of the antenna (set to 50 Ω). Ideally, when $\Delta \to 0$, the two devices behave in the same fashion. However, due to frequency mismatch between the array elements, an attenuated peak arises around $f_s$, while $\bar{f}_{RF}$ slighly differs from $f_{RF}$ (Fig.7). As expected, no gain attenuation is recorded for the array of mismatched elements thanks to the capacitive coupling.

## V. Conclusions

In this paper, a coupling technique to eliminate the impact of frequency mismatch in arrays of MEMS resonators is demonstrated via analytical modeling, numerical simulations, and direct measurement of coupled devices. The technique exploits a series capacitor to induce poles coupling and it is insensitive to the number of arrayed elements or their $FoM$.

## References


[1] R. Ruby, "A snapshot in time: The future in filters for cell phones," *IEEE Microwave Magazine*, vol. 16, pp. 46–59, aug 2015.

[2] M. D. Williams, B. A. Griffin, T. N. Reagan, J. R. Underbrink, and M. Sheplak, "An AlN MEMS piezoelectric microphone for aeroacoustic applications," *Journal of Microelectromechanical Systems*, vol. 21, pp. 270–283, apr 2012.

[3] D. K. Shaeffer, "MEMS inertial sensors: A tutorial overview," *IEEE Communications Magazine*, vol. 51, no. 4, pp. 100–109, 2013.

[4] C. S. Lam, "A review of the recent development of mems and crystal oscillators and their impacts on the frequency control products industry," *Proceedings - IEEE Ultrasonics Symposium*, pp. 694–704, 2008.

[5] G. Zhanshe, C. Fucheng, L. Boyu, C. Le, L. Chao, and S. Ke, "Research development of silicon MEMS gyroscopes: a review," *Microsystem Technologies*, vol. 21, pp. 2053–2066, oct 2015.

[6] Y. Lu, H. Tang, S. Fung, Q. Wang, J. M. Tsai, M. Daneman, B. E. Boser, and D. A. Horsley, "Ultrasonic fingerprint sensor using a piezoelectric micromachined ultrasonic transducer array integrated with complementary metal oxide semiconductor electronics," *Applied Physics Letters*, vol. 106, p. 263503, jun 2015.

[7] L. Colombo, M. E. Galanko Klemash, T. M. Kiebala, S. S. Bedair, G. Piazza, and M. Rinaldi, "VHF and UHF Lithium Niobate MEMS Resonators Exceeding 30 dB of Passive Gain," *IEEE Electron Device Letters*, vol. 42, pp. 1853–1856, Dec 2021.

[8] L. Colombo, A. Kochhar, G. Vidal-Alvarez, and G. Piazza, "High Figure of Merit X-cut Lithium Niobate MEMS Resonators Operating Around 50 MHz for Large Passive Voltage Amplification in Radio Frequency Applications," *IEEE Transactions on Ultrasonics, Ferroelectrics, and Frequency Control*, p. 1, Feb. 2020.

[9] L. Colombo, A. Kochhar, G. Vidal-Álvarez, and G. Piazza, "Impact of Frequency Mismatch on the Quality Factor of Large Arrays of X-Cut Lithium Niobate MEMS Resonators," *Journal of Microelectromechanical Systems*, vol. 29, pp. 1455–1463, Dec. 2020.

[10] G. Piazza and H. Bhugra, eds., *Piezoelectric MEMS Resonators*. Microsystems and Nanosystems, Springer International Publishing, 2017.

[11] P. Bassirian, J. Moody, R. Lu, A. Gao, T. Manzaneque, A. Roy, N. Scott Barker, B. H. Calhoun, S. Gong, and S. M. Bowers, "Nanowatt-Level Wakeup Receiver Front Ends Using MEMS Resonators for Impedance Transformation," *IEEE Transactions on Microwave Theory and Techniques*, vol. 67, pp. 1615–1627, Apr. 2019.